

Article

Slope Failure Risk Assessment Considering Both the Randomness of Groundwater Level and Soil Shear Strength Parameters

Pu Peng¹, Ze Li^{1,*}, Xiaoyan Zhang¹, Wenlian Liu², Sugang Sui² and Hanhua Xu³

¹ Faculty of Civil Engineering and Mechanics, Kunming University of Science and Technology, Kunming 650500, China; 20182110047@stu.kust.edu.cn (P.P.); zhangxiaoyan@kust.edu.cn (X.Z.)

² Kunming Prospecting Design Institute, China Nonferrous Metals Industry Co., Ltd., Kunming 650051, China; lwenl702@sina.com (W.L.); suisugang2@zskk1953.com (S.S.)

³ Yunnan Key Laboratory of Geotechnical Engineering and Geohazards, Kunming 650051, China; xuhanhua@zskk1953.com

* Correspondence: lize@kust.edu.cn; Tel.: +86-15974807239

Abstract: Conducting research on slope failure risk assessment is beneficial for the sustainable development of slopes. There will be various failure modes considering both the randomness of the groundwater level and soil shear strength parameters. Based on the integrated failure probability (IFP), the traditional failure risk analysis needs to count all failure modes, including the failure probability (P_f) and failure risk coefficient (C), one-by-one. A new slope failure risk assessment method that uses the sum of the element failure risk to calculate the overall failure risk is proposed in this paper and considers both the randomness of the groundwater level and soil shear strength parameters. The element failure probability is determined by their location information and failure situation; the element failure risk coefficient is determined by their area. It transforms the complex overall failure risk problem into a simple element failure risk problem, which simplifies the calculation process and improves the calculation efficiency greatly. The correctness is verified with the systematic analysis of a classical case. The results show that the slope failure probability and failure risk are greatly increased from 1.40% to 3.30% and 0.829 m² to 2.094 m² with rising groundwater level, respectively.

Keywords: failure risk; element failure probability; spatial variability; stochastic groundwater level; upper bound method



check for updates

Citation: Peng, P.; Li, Z.; Zhang, X.; Liu, W.; Sui, S.; Xu, H. Slope Failure Risk Assessment Considering Both the Randomness of Groundwater Level and Soil Shear Strength Parameters. *Sustainability* **2023**, *15*, 7464. <https://doi.org/10.3390/su15097464>

Academic Editor: Jianjun Ma

Received: 9 April 2023

Revised: 26 April 2023

Accepted: 28 April 2023

Published: 1 May 2023



Copyright: © 2023 by the authors. Licensee MDPI, Basel, Switzerland. This article is an open access article distributed under the terms and conditions of the Creative Commons Attribution (CC BY) license (<https://creativecommons.org/licenses/by/4.0/>).

1. Introduction

There are many factors that induce slope instability, among which the influences of the mechanical parameters of soil mass and groundwater are particularly important [1]. Due to long-term geological actions, such as sedimentation, post-sedimentation, chemical weathering, and physical denudation, the mechanical parameters of natural soil show certain spatial variability, which affects both the safety performance and failure mode of a slope. However, these effects are often ignored in practical engineering [2,3]. Groundwater mainly affects the safety performance from two aspects: one is making the seepage field change, affecting the stability performance; and the other is reducing shear strength parameters, affecting the safety performance [4]. Generally, the groundwater level inside the slope is not a certain value and is influenced by various uncertain factors. Therefore, it is essential to establish a failure risk analysis model of soil slopes that considers both the spatial variability and the stochasticity of the groundwater level so as to simulate the slope more in line with the real situation and achieve sustainable development of the slope.

In recent years, the slope reliability problem under consideration of spatial variability has received widespread attention by researchers. Using the limit equilibrium method (LEM), the probability density function (PDF) curve and cumulative probability density function (CDF) curve of the safety factor can be acquired directly by first assuming the

sliding surface. However, the LEM only takes the one-dimensional spatial variability of the soil material into account and ignores the impact outside the sliding surface on the slope reliability. In addition, the LEM does not consider the constitutive relation of the soil, so the stress–strain relationship cannot be acquired [5–11]. Using the finite element method (FEM) without assuming the sliding surface, the constitutive relation and spatial variability of materials can be fully considered so as to obtain more reasonable calculation results compared with the LEM [12]. In addition, the FEM can analyze the stress–strain development and progressive slope failure process, but the calculation cost is high [12–16]. Using the limit analysis method (LAM), the range of true solutions and corresponding failure modes can be acquired efficiently and accurately with the upper bound method (UBM) and lower bound method (LBM) [17–24]. Chen Zhaohui et al. combined the stochastic FEM and LAM, taking the spatial variability into account for the slope reliability analysis, and gave the strict frequency distribution range of the safety factor [25]. Peng Pu et al. carried out a study on element failure probability and used affinity propagation (AP) cluster analysis to obtain the failure modes of soil slope [26]. The above research greatly promotes the application prospect of the LAM in slope reliability analysis; however, it is not always reasonable to use only the failure probability to evaluate the slope. For example, there are two failure modes of a slope, corresponding to shallow landslide (P_{f1}, C_1) and deep landslide (P_{f2}, C_2). P_{f1} is larger than P_{f2} , but C_1 is smaller than C_2 , so which failure mode has greater impact? To fully consider the impact of P_f and C , researchers proposed the concept of slope failure risk (R) [27,28]. However, whether we use the LEM or FEM to calculate the slope failure risk, the failure modes of the slope need to be identified and counted first, and there is lower computational efficiency with large sample calculations. Zhang Xiaoyan et al., using the slope safety factor and velocity field information to calculate the element failure probability (EFP), provide a new idea for the calculation of slope failure risk [29].

Currently, the groundwater level is usually defaulted at a certain value, and the limit state function does not contain the groundwater level as a stochastic variable. However, due to the stochastic distribution of soil particles and pores inside the slope, the seepage field is uncertain. In addition, because of the uncertainty of the supply by precipitation, surface runoff, underground confluence, and the discharge by evaporation and pumping, the groundwater level is uncertain. It is well known that the groundwater level is directly related to the seepage field, so the stochastic groundwater level will lead to the uncertainty of the seepage field. In recent years, the research about the seepage field mainly focused on the change in the permeability coefficient and paid less attention to the stochastic groundwater level, which leads to the change in the seepage field [30,31]. In addition, autocorrelation functions, such as exponential, Gaussian, logarithmic, and triangular, are frequently applied to characterize the spatial variability of soil mass [32]. In view of this, a slope failure risk assessment method that considers both the randomness of the groundwater level and soil shear strength parameters is proposed in this paper to achieve sustainable development.

2. Methodologies

2.1. Stable Seepage Field of Slope with Stochastic Groundwater Level

In this paper, a slope failure risk assessment that considers both the randomness of the groundwater level and soil shear strength parameters is carried out. Figure 1 shows the stochastic groundwater level model for soil slopes, which includes the velocity of the triangular element, the model of the groundwater level distribution, the shear strength parameters' calculation, and the pore water pressure calculation. The soil mass is discretized by the triangular element, so the three nodes of the element e have horizontal velocity u_i^e , vertical velocity v_i^e , cohesive force c_i^e , friction angle φ_i^e , and pore water pressure p_i^e , of which $i = (1, 2, 3)$ and $e = (1, \dots, N_e)$. In addition, there is discontinuity between element a and element b . Nodes ① and ② belong to element a ; Nodes ② and ④ belong to element b .

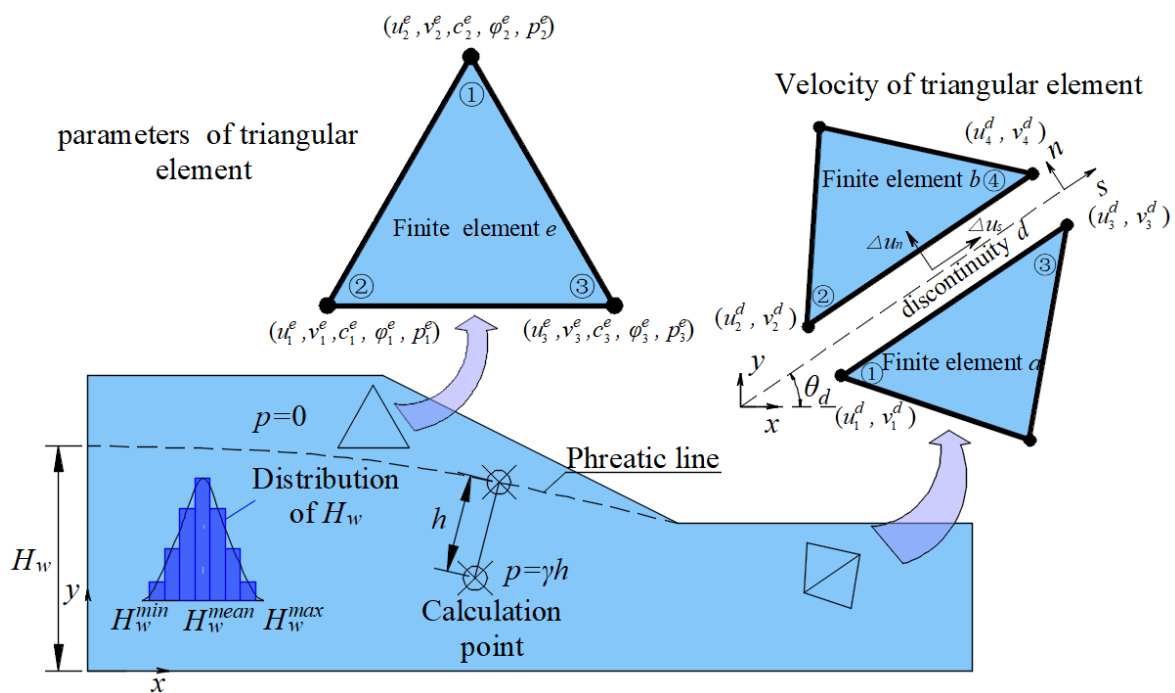


Figure 1. Stochastic groundwater level model for soil slope.

Similar to the literature [33], it is assumed that the stochastic groundwater level H_w follows a truncated normal distribution, where H_w^{min} is the left-truncated tail of the stochastic groundwater level, H_w^{max} is the right-truncated tail of the stochastic groundwater level, and H_w^{mean} is the mean value of the stochastic groundwater level. In addition, this article makes the following assumptions: (1) the seepage field is a saturated and stable seepage field; (2) excess pore water pressure along with the effect on the soil shear strength parameters caused by a sudden rise or drop of groundwater level are not considered; (3) above the phreatic line, the pore water pressure is $p = 0$; and (4) below the phreatic line, the pore water pressure is $p = \gamma h$, of which γ is the volume weight of water, and h is the vertical distance from the point on the phreatic line that is on the same equipotential line as the calculation point to the calculation point. The two-dimensional stable seepage equation is used for the seepage analysis [31]. The specific equation is as follows:

$$k_x \frac{\partial^2 H_w}{\partial x^2} + k_y \frac{\partial^2 H_w}{\partial y^2} = 0 \tag{1}$$

where k_x and k_y are the permeability coefficient in the x and y direction, respectively; and H_w is the stochastic groundwater head function at each point within the soil.

2.2. Stochastic Field of Parameter Spatial Variability

Considering that slope reliability is sensitive to autocorrelation length and insensitive to the form of the autocorrelation function [34,35], this paper selects the exponential autocorrelation function with a simpler mathematical expression for research, which can be expressed with the following equation [35]:

$$\rho[(x_a, y_a); (x_b, y_b)] = \exp \left[-2 \left(\frac{x_a - x_b}{L_h} \right) - 2 \left(\frac{y_a - y_b}{L_v} \right) \right] \tag{2}$$

where $x_a, y_a, x_b,$ and y_b are the coordinate components of the spatial coordinates; and L_h and L_v are the fluctuation range in the x and y direction, respectively.

Due to the existence of certain mutual correlations between soil parameters and certain autocorrelations of the soil parameters themselves thus involving the discrete process

of the associated non-Gaussian fields, this paper adopts a method similar to that of the literature [35] using the midpoint method of Cholesky decomposition for the stochastic field generation, and for the exponential autocorrelation functions, the associated logarithmic stochastic field of the soil materials is as follows:

$$c_i^e = \exp(u_{\ln c} + \sigma_{\ln c} \cdot c_i^{eD}) \quad (3)$$

$$\varphi_i^e = \exp(u_{\ln \varphi} + \sigma_{\ln \varphi} \cdot \varphi_i^{eD}) \quad (4)$$

where c_i^e and φ_i^e are the soil cohesion and internal friction angle of nodes i upon element e in the non-Gaussian stochastic field, respectively; c_i^{eD} and φ_i^{eD} are the soil cohesion and internal friction angle of nodes i upon element e in the Gaussian stochastic field, respectively; $\sigma_{\ln c} = \sqrt{\ln(1 + (\sigma_c^2/u_c^2))}$; $\sigma_{\ln \varphi} = \sqrt{\ln(1 + (\sigma_\varphi^2/u_\varphi^2))}$; $u_{\ln c} = \ln u_c - \sigma_{\ln c}^2/2$; $u_{\ln \varphi} = \ln u_\varphi - \sigma_{\ln \varphi}^2/2$; u_c and σ_c are the mean and standard deviation of the log-normal distribution of c , respectively; u_φ and σ_φ are the mean and standard deviation of the log-normal distribution of φ , respectively; $u_{\ln c}$ and $\sigma_{\ln c}$ are the mean and standard deviation of the corresponding normal variable of $\ln c$, respectively; and $u_{\ln \varphi}$ and $\sigma_{\ln \varphi}$ are the mean and standard deviation of the corresponding normal variable of $\ln \varphi$, respectively.

2.3. Stochastic Programming Model

Sloan et al. [20] discretized the soil mass with triangular elements (as shown in Figure 1) and constructed the kinematically admissible velocity fields (KAVF). It is easy to discern from the UBM that the KAVF is one-to-one, corresponding to the external load, where the minimum is infinitely close to the limit load; therefore, the UBM can be understood for solving the minimization problem. On the basis of previous studies [20,26,29,36], the stochastic programming model that considers both the randomness of the groundwater level and soil shear strength parameters established in this paper is as follows:

$$\begin{cases} Z = k_m - 1 \\ \text{Minimize : } k_\gamma = \mathbf{W}_e + \mathbf{W}_d - \mathbf{W}_e^p - \mathbf{W}_d^p \\ \text{Subject to : } \mathbf{a}_e^1 \mathbf{u}_e - \mathbf{a}_e^2 \chi_e = 0 \\ \mathbf{a}_d^1 \mathbf{u}_d - \mathbf{a}_d^2 \chi_d = 0 \\ \mathbf{a}_b \mathbf{u}_b = 0 \\ \mathbf{W}_G = 1; \chi_e \geq 0; \chi_d \geq 0 \end{cases} \quad (5)$$

where Z is the limit state function; k_m and k_γ are the safety factor and volume weight overload factor, respectively; χ_e and χ_d are the plastic multiplier of finite element e and node d , respectively; \mathbf{a}_e^1 , \mathbf{a}_e^2 and \mathbf{a}_d^1 , \mathbf{a}_d^2 are the plastic flow constraint matrix of the finite element e and velocity discontinuity d , respectively; $\mathbf{u}_e = [u_1^e \ v_1^e \ u_2^e \ v_2^e \ u_3^e \ v_3^e]^T$, of which u_i^e and v_i^e are the horizontal and vertical velocity components of nodes i upon element e , respectively; $\mathbf{u}_d = [u_1^d \ v_1^d \ u_2^d \ v_2^d \ u_3^d \ v_3^d \ u_4^d \ v_4^d]^T$, of which u_i^d and v_i^d are the horizontal and vertical velocity components of nodes i upon velocity discontinuity d , respectively; $\mathbf{a}_b = \begin{bmatrix} \cos \theta & \sin \theta \\ -\sin \theta & \cos \theta \end{bmatrix}$, of which θ is the rotation angle; $\mathbf{u}_b = [u_1^b \ v_1^b \ K \ K \ u_j^b \ v_j^b]$, of which u_j^b and v_j^b are the horizontal and vertical velocity components on the boundary, respectively; \mathbf{W}_e and \mathbf{W}_d are the internal power of finite element e and velocity discontinuity d , respectively; \mathbf{W}_e^p and \mathbf{W}_d^p are the external power of finite element e and velocity discontinuity d , respectively; and \mathbf{W}_G is the external power of self-weight [20].

3. Solution Strategy

The \mathbf{a}_e^2 , \mathbf{a}_d^2 , \mathbf{W}_e , \mathbf{W}_d , \mathbf{W}_e^p , and \mathbf{W}_d^p matrices in Equation (5) are all associated with the groundwater level as well as the shear strength parameters. Currently, there is no

better method for solving this kind of problem; in view of this, on the basis of the Monte Carlo simulation, an iterative method is proposed for solving this issue. The detailed implementation process is as follows:

- (1) Assuming that the stochastic groundwater level follows a truncated normal distribution, which is generated with the Monte Carlo simulation method:

$$\begin{cases} H_w(T_w) = \text{Random}(\text{Normal}, \mu_w, \sigma_w, 1, N_w) \\ H_w^{\min} \leq H_w(T_w) \leq H_w^{\max} \end{cases} \quad (6)$$

where $H_w(T_w)$ is the T_w th groundwater level; $T_w = (1, \dots, N_w)$, N_w is the number of groundwater level; and μ_w and σ_w are the mean and standard deviation of the groundwater level, respectively.

- (2) Assuming that the autocorrelation functions of the soil materials are exponential type, using Equations (3) and (4), the midpoint method of Cholesky decomposition for the stochastic field generation $c^e(T_m)$ and $\varphi^e(T_m)$, of which $T_m = (1, \dots, N_m)$; N_m is the number of random fields for the shear strength parameters.

In this paper, the slope is allowed to reach the limit state by means of capacitive overload, and the capacitive overload factor of the slope when taking the parameters' spatial variability into account under the effect of the stochastic groundwater level is as follows:

$$k_\gamma(T_m, T_w) = \frac{\gamma_c(c^e(T_m), \varphi^e(T_m), H_w(T_w))}{\gamma_a} \quad (7)$$

where $k_\gamma(T_m, T_w)$ is the capacitive overload factor; $\gamma_c(c^e(T_m), \varphi^e(T_m), H_w(T_w))$ is the capacity of the soil in the ultimate state, which is related to $c^e(T_m)$, $\varphi^e(T_m)$, and $H_w(T_w)$; and γ_a is the actual capacity of the soil.

The slope safety factor when taking the parameters' spatial variability into account under the effects of the stochastic groundwater level is as follows:

$$k_m(T_m, T_w) = \frac{c^e(T_m)}{c'^e(T_m)} = \frac{\varphi^e(T_m)}{\varphi'^e(T_m)} \quad (8)$$

where $k_m(T_m, T_w)$ is the safety factor; and $c'^e(T_m)$ and $\varphi'^e(T_m)$ are the cohesion and internal friction angle of finite element e in the T_m th non-Gaussian stochastic field after the strength reduction, respectively.

- (3) The stochastic number of T_w groundwater levels generated in step (1) is substituted into the stable seepage field calculation equation to obtain the pore water pressure $p_1^e(T_w)$, $p_2^e(T_w)$, $p_3^e(T_w)$; $e = (1, \dots, N_e)$; $T_w = (1, \dots, N_w)$.
- (4) From $T_w = 1$ to $T_w = N_w$ cycles, repeat $p_1^e(T_w)$, $p_2^e(T_w)$, $p_3^e(T_w)$, all the finite element nodes' pore water pressure values are successively replaced with the stochastic programming model for the slope reliability analysis; in each cycle from $T_w = 1$ to $T_w = N_w$; $c^e(T_m)$, $\varphi^e(T_m)$ from $T_m = 1$ to $T_m = N_m$ cycles, the number of N_m stochastic fields are brought into Equation (5) and use the dual simplex method to obtain $N_w \times N_m$ numbers of capacity overload factors [$k_\gamma(T_m, T_w)$] while, at the same time, use the bisection method to obtain $N_w \times N_m$ numbers of the slope safety factor [$k_m(T_m, T_w)$]. Figure 2 shows the specific numerical solution flow.
- (5) Calculation of the slope safety factor and plot the related curve.

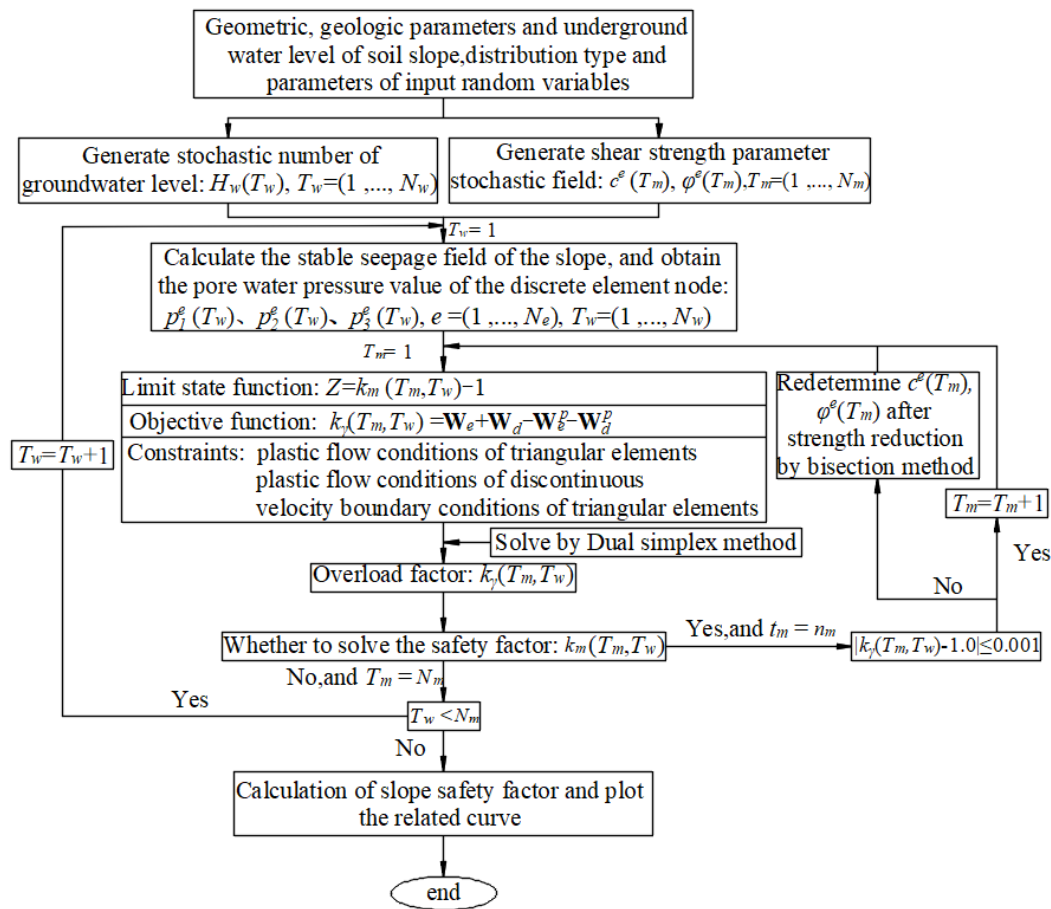


Figure 2. Specific numerical solution flow for slope.

4. Reliability Index for Slope

The traditional *IFP* uses the threshold value of the safety factor to determine whether the slope will fail or not and then conducts the slope reliability analysis accordingly [28]. Based on the *IFP*, the slope failure function is as follows:

$$I(T_m, T_w) = \begin{cases} 0, & \text{if } k_m(T_m, T_w) \geq 1 \\ 1, & \text{if } k_m(T_m, T_w) < 1 \end{cases} \quad (9)$$

where $I(T_m, T_w)$ is the failure function of the slope corresponding to the T_m th stochastic field under T_w th groundwater level acts.

According to the Equation (8) slope failure function, the *IFP* under T_w th groundwater level acts can be acquired as follows:

$$P_f^{IFP}(T_w) = \frac{\sum_{T_m=1}^{N_m} I(T_m, T_w)}{N_m} \times 100\% \quad (10)$$

where $P_f^{IFP}(T_w)$ is the *IFP* of the slope under T_w th groundwater level acts.

Further, the *IFP* of the slope is as follows:

$$P_f^{IFP} = \sum_{T_w=1}^{N_w} P_f^{IFP}(T_w) \quad (11)$$

where P_f^{IFP} is the *IFP* of the slope under all potential groundwater level acts.

The integrated failure risk (*IFR*) of the slope under T_w th groundwater level acts is as follows:

$$R^{IFP}(T_w) = P_f^{IFP}(T_w)C \quad (12)$$

where $R^{IFP}(T_w)$ is the *IFR* of the slope under T_w th groundwater level acts, and C is the area of the slope failure mode.

Based on the *IFP*, the *IFR* of the slope is calculated as follows [27,28]:

$$R^{IFP} = \sum_{T_w=1}^{N_w} R^{IFP}(T_w) \quad (13)$$

where R^{IFP} is the *IFR* of the slope.

The Equation (13) default is that only one failure mode exists when conducting the slope failure risk analysis, which is contrary to the fact that slopes have multiple failure modes, considering both the randomness of the groundwater level and soil shear strength parameters. For that reason, Huang et al. [37] gave a calculation equation, which considered all failure modes of the slope simultaneously as follows:

$$R_k^{IFP}(T_w) = P_{fk}^{IFP}(T_w)C_k \quad (14)$$

where $R_k^{IFP}(T_w)$ is the *IFR* of the k th failure mode of the slope under T_w th groundwater level acts; $P_{fk}^{IFP}(t_w)$ is the *IFP* of the k th failure mode of the slope under T_w th groundwater level acts; and C_k is the area of the k th slope failure mode.

The *IFR* of the slope is as follows:

$$R^{IFP} = \sum_{T_w=1}^{N_w} \sum_{k=1}^N R_k^{IFP}(T_w) \quad (15)$$

Compared with Equations (13) and (15), it can perform both single and multiple failure mode slope risk assessments; however, both the LEM and FEM require prior work on complex failure mode classification. Zhang Xiaoyan et al. [29] proposed a new concept of *EFP* on the basis of the UBM. They used the slope safety factor and the KVAF to judge the failure elements. The failure function, considering the stochasticity of the groundwater level and spatial variability of soil material, is as follows:

$$I_e(T_m, T_w) = \begin{cases} 0 & \text{if } k_m(T_m, T_w) \geq 1 \\ 0 & \text{if } u_c^e(T_m, T_w) = 0 \text{ and } k_m(T_m, T_w) < 1 \\ 1 & \text{if } u_c^e(T_m, T_w) > 0 \text{ and } k_m(T_m, T_w) < 1 \end{cases} \quad (16)$$

where $I_e(T_m, T_w)$ is the failure function of the element e corresponding to the T_m th stochastic field under T_w th groundwater level acts, and $u_c^e(T_m, T_w)$ is the velocity of the element e corresponding to the T_m th stochastic field under T_w th groundwater level acts.

$$u_c^e(T_m, T_w) = \sqrt{\left(\sum_{i=1}^3 \frac{u_i^e(T_m, T_w)}{3}\right)^2 + \left(\sum_{i=1}^3 \frac{v_i^e(T_m, T_w)}{3}\right)^2} \quad (17)$$

where $u_i^e(T_m, T_w)$ is the horizontal velocity component of nodes i upon element e corresponding to the T_m th stochastic field under T_w th groundwater level acts, and $v_i^e(T_m, T_w)$ is the vertical velocity component of nodes i upon element e corresponding to the T_m th stochastic field under T_w th groundwater level acts.

According to the slope element failure function in Equation (16), the slope element failure probability (*EFP*) under T_w th groundwater level acts is as follows:

$$P_{fe}^{EFP}(T_w) = \frac{\sum_{T_m=1}^{N_m} I^e(T_m, T_w)}{N_m} \times 100\% \quad (18)$$

where $P_{fe}^{EFP}(T_w)$ is the *EFP* under T_w th groundwater level acts.

The slope *EFP* under all potential groundwater level acts is as follows:

$$P_{fe}^{EFP} = \frac{\sum_{T_w=1}^{N_w} \sum_{T_m=1}^{N_m} I^e(T_m, T_w)}{N_w \times N_m} \times 100\% \quad (19)$$

The element failure risk (*EFR*) of the slope under T_w th groundwater level acts is as follows:

$$R_e^{EFP}(T_w) = P_{fe}^{EFP}(T_w)C_e \quad (20)$$

where $R_e^{EFP}(T_w)$ is the failure risk of element e under T_w th groundwater level acts, and C_e is the area of element e .

The element failure risk (*EFR*) of the slope under all potential groundwater level acts is as follows:

$$R_e^{EFP} = \sum_{T_w=1}^{N_w} R_e^{EFP}(T_w) \quad (21)$$

where R_e^{EFP} is the failure risk of element e under all potential groundwater level acts.

The *IFR* based on the *EFP* of the slope under T_w th groundwater level acts is calculated in the following equation [20]:

$$R^{EFP}(T_w) = \sum_{e=1}^{N_e} R_e^{EFP}(T_w) \quad (22)$$

where $R^{EFP}(T_w)$ is the *IFR* under T_w th groundwater level acts.

The *IFR* based on the *EFP* of the slope under all potential groundwater level acts is calculated in the following equation:

$$R^{EFP} = \sum_{T_w=1}^{N_w} R^{EFP}(T_w) \quad (23)$$

where R^{EFP} is the *IFR* under all potential groundwater level acts.

A new slope failure risk assessment under consideration of the stochastic groundwater level involves *EFP* and C_e . The *EFP* can be easily obtained by solving the stochastic programming model, and C_e is the area of element e , which is constant compared to C_k .

According to the solution strategy of the stochastic programming model, the $N_w \times N_m$ slope safety factors $k_m(T_m, T_w)$ can be easily acquired. Using statistical knowledge, the mean and standard deviation of the slope safety factor can be calculated as follows:

$$\mu_k(T_w) = \frac{\sum_{T_m=1}^{N_m} k_m(T_m, T_w)}{N_m} \quad (24)$$

$$\mu_k = \frac{\sum_{T_w=1}^{N_w} \sum_{T_m=1}^{N_m} k_m(T_m, T_w)}{(N_w \times N_m)} \quad (25)$$

$$\sigma_k(T_w) = \sqrt{\frac{\sum_{T_m=1}^{N_m} (k_m(T_m, T_w) - \mu_k(T_w))^2}{N_m - 1}} \tag{26}$$

$$\sigma_k = \sqrt{\frac{\sum_{T_w=1}^{N_w} \sum_{T_m=1}^{N_m} (k_m(T_m, T_w) - \mu_k)^2}{N_w \times N_m - 1}} \tag{27}$$

where $T_w = (1, \dots, N_w)$; $\mu_k(T_w)$ and $\sigma_k(T_w)$ are the mean and standard deviation of the slope safety factor under T_w th groundwater level acts, respectively; and μ_k and σ_k are the mean and standard deviation of the slope safety factor under all potential groundwater level acts, respectively.

5. Calibration and Application

The UBM program is compiled, and a classic slope calculation example is calculated and analyzed. Comparing the result with the calculation result of the LEM, we verified the correctness of the calculation method.

5.1. Numerical Simulations

Figure 3 shows the homogeneous slope calculation model. The height is 5 m, the width of the top is 10 m, and the ratio is 1:2. Li Dian qing et al. have calculated the failure probability of the slope [35] but have not conducted systematic research on the slope failure risk. In view of this, on the basis of the method proposed in this paper, the slope failure risk is studied. Using the triangular element to discretize the slope, 989 finite elements, 2967 nodes, and 1536 discontinuities are acquired. In addition, there are three pore water pressure monitoring points: P1 (5,5), P2 (10,5), and P3 (15,5). The set soil volume weight γ is 20.0 kN/m³, and the permeability coefficient is $K = 5 \times 10^{-7}$ m/s, both of which are determined values. See Table 1 for the other calculation parameters [26].

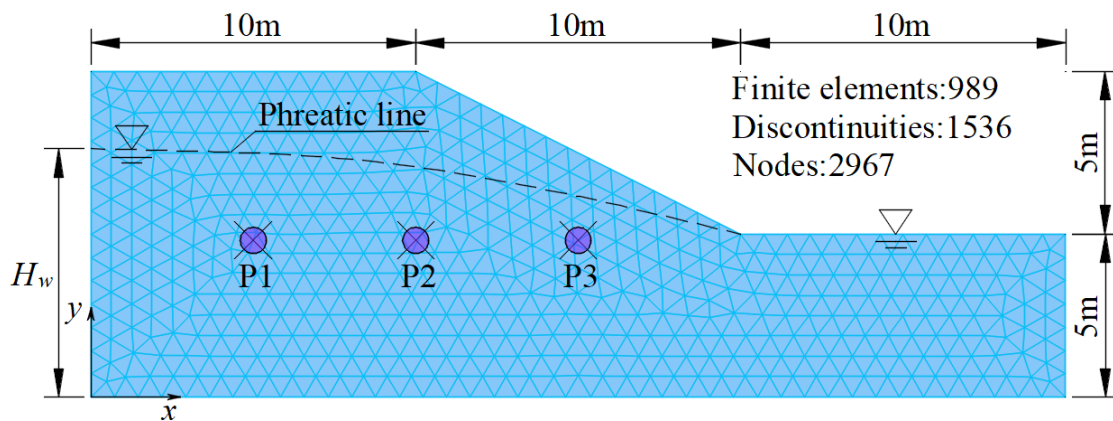


Figure 3. Homogeneous slope calculation model.

Table 1. Statistics of the soil parameters.

Shear Parameter	Mean	Correlation of Variation	Distribution Type	Fluctuation Range	Correlation Coefficient
c (kPa)	10	0.3	Lognormal	$L_h = 40$ m	$\rho_{c,\varphi} = -0.5$
φ (°)	30	0.2	Lognormal	$L_v = 4$ m	

The mean and standard deviation of the stochastic groundwater level is 7.5 m and 2.25, respectively, on the basis of the measured groundwater in many projects. The upper boundary of the groundwater level is 8.5 m. The lower boundary of the groundwater level is 6.5 m. The quantity of the stochastic groundwater levels is 50. The groundwater level at

the right slope toe is 5 m. According to Equation (6), 50 stochastic numbers of groundwater levels are generated, and their distribution is shown in Figure 4. The stochastic number distribution of the groundwater is relatively close to the mean value of the groundwater level, and relatively small near the relatively high and low groundwater levels.

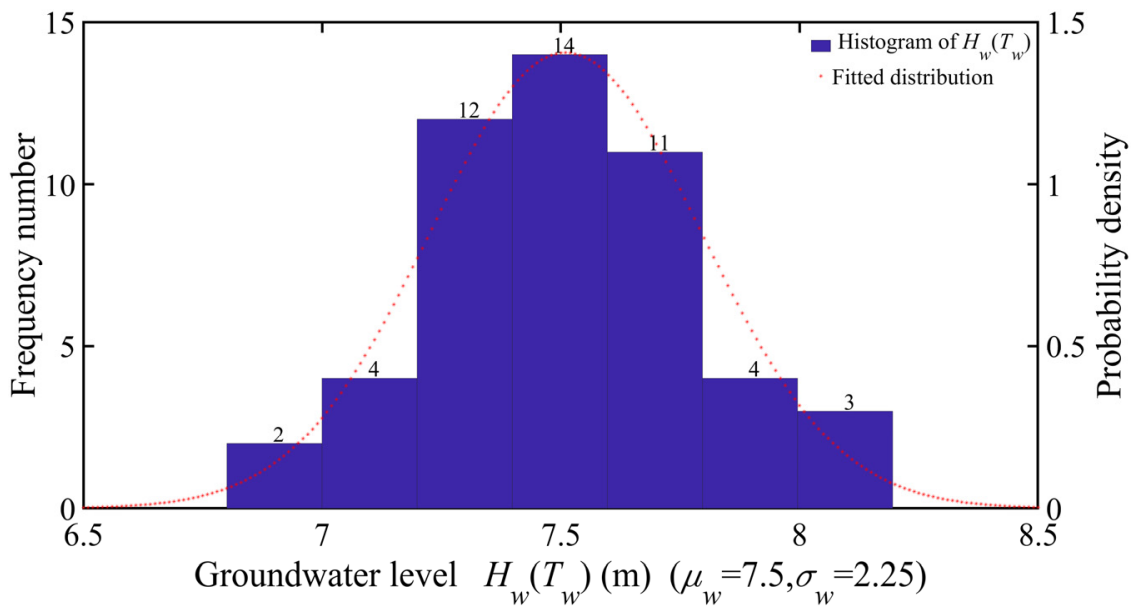


Figure 4. Stochastic groundwater levels distribution histogram.

Figure 5a–c shows the slope stable seepage fields when $T_w = 1$ ($H_w = 6.8006$ m), $T_w = 25$ ($H_w = 7.4848$ m), and $T_w = 50$ ($H_w = 8.1951$ m), respectively. It can be observed that the contours of the pore water pressure become steeper, and the saturated area inside the slope increases as the groundwater level rises. Figure 6 shows the key points pore water pressure. Under the same groundwater level act, the pore water pressure decreases gradually as the coordinates of the key points move to the right. At P1, the mean and standard deviation of the pore water pressure are -19.77 kPa and 2.31 kPa, respectively. At P2, the mean and standard deviation of the pore water pressure are -14.59 kPa and 1.78 kPa, respectively. At P3, the mean and standard deviation of the pore water pressure are -8.94 kPa and 1.13 kPa, respectively.

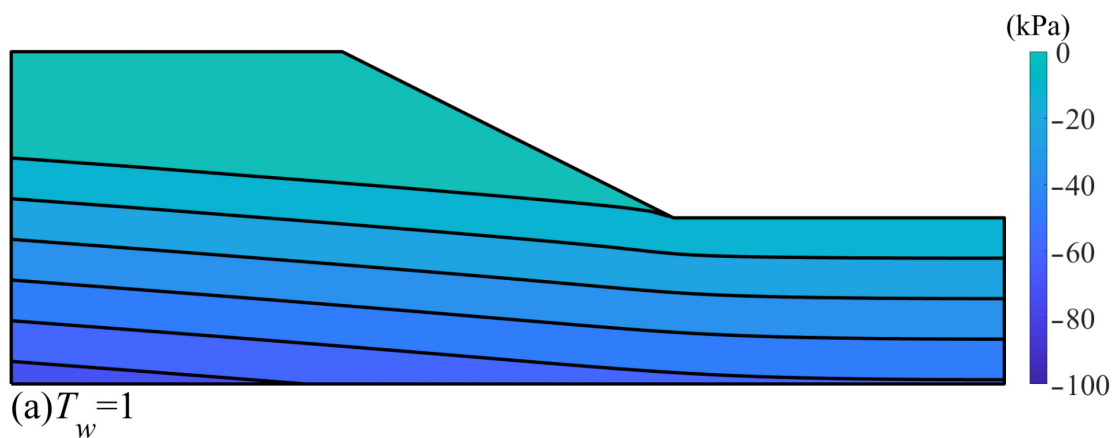


Figure 5. Cont.

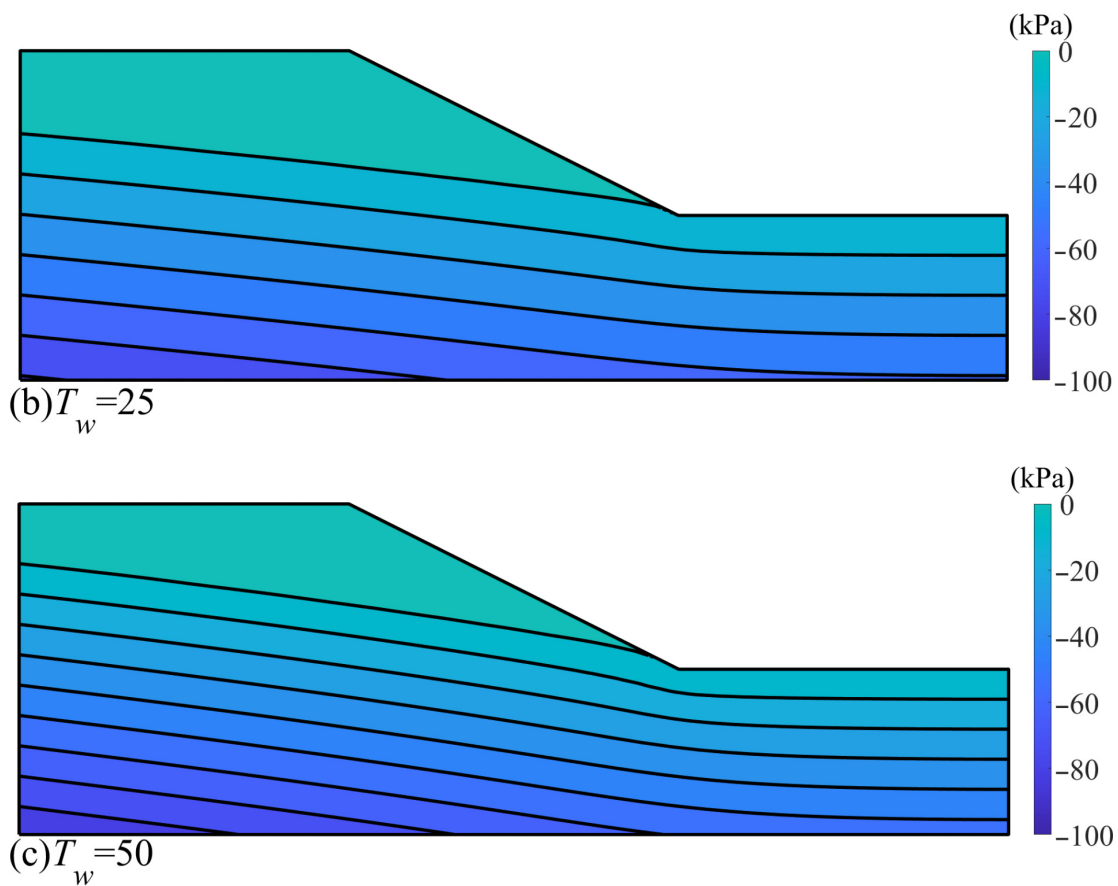


Figure 5. Steady seepage fields of slope: (a) $T_w = 1$; (b) $T_w = 25$; (c) $T_w = 50$.

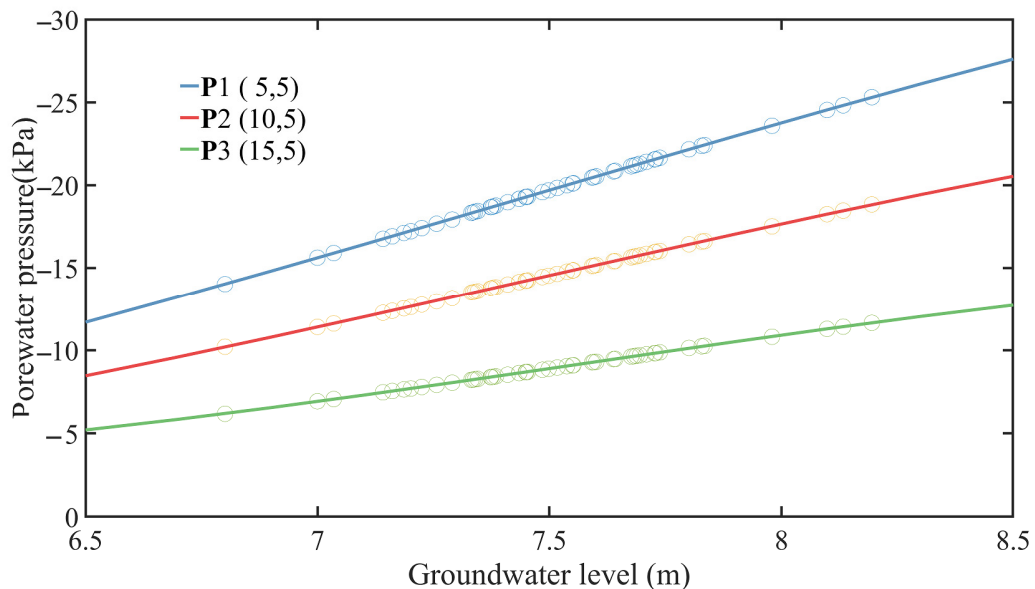


Figure 6. The key points pore water pressure.

Assuming that the autocorrelation functions of the soil materials are exponential type, we used the midpoint method of Cholesky decomposition for the stochastic field generation. The quantity of the stochastic fields of the soil parameters is 2000; according to Equations (3) and (4), 2000 stochastic fields of the slope shear strength parameters are generated. Figure 7a,b shows the stochastic fields of $c_e(500)$ and $\varphi_e(500)$, respectively. The

maximum value of soil cohesion and internal friction angle are 18.9084 kPa and 23.3219°, respectively; The minimum value of soil cohesion and internal friction angle are 3.1696 kPa and 9.5851°, respectively. In addition, soil cohesion has a certain negative correlation with internal friction angle in space.

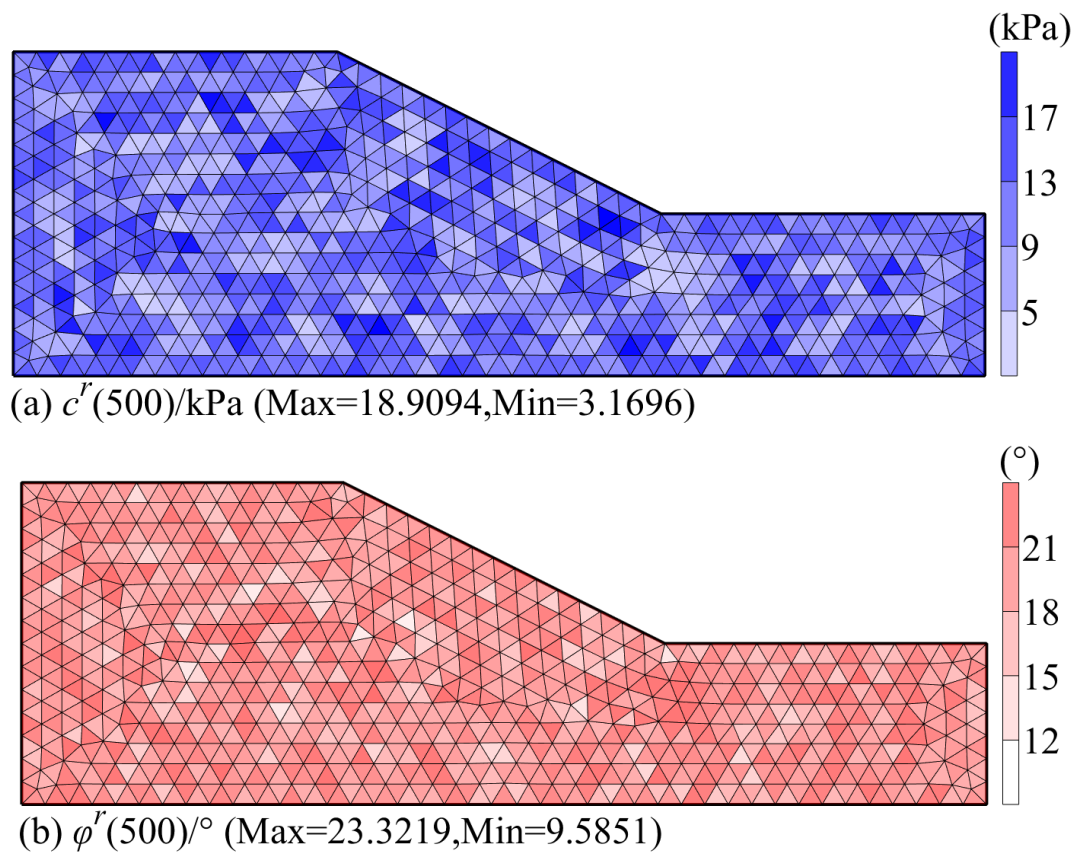


Figure 7. Stochastic fields of the slope shear strength parameters: (a) $c^r(500)$; (b) $\varphi^r(500)$.

5.2. Main Results of the Research

This paper selects low, medium, and high groundwater levels ($T_w = 1$, $T_w = 25$, and $T_w = 50$) for comparative analysis to verify the effectiveness of the calculation method. Table 2 shows the calculation results of the reliability index comparison between the UBM and LEM under three groundwater level acts: $T_w = 1$, $T_w = 25$, and $T_w = 50$. Figure 8 shows the distribution characteristics of the slope safety factor under three groundwater level acts. Figure 9 shows the distribution histograms of the slope safety factor under three groundwater level acts.

Table 2. Calculation results of the reliability index.

Groundwater Level	Method	Mean	Standard Deviation	Failure Probability (%)
$T_w = 1$	UBM	1.2956	0.1420	1.40
	LEM	1.2923	0.1488	1.90
$T_w = 25$	UBM	1.2678	0.1394	2.10
	LEM	1.2622	0.1461	2.70
$T_w = 50$	UBM	1.2357	0.1365	3.30
	LEM	1.2310	0.1432	4.65

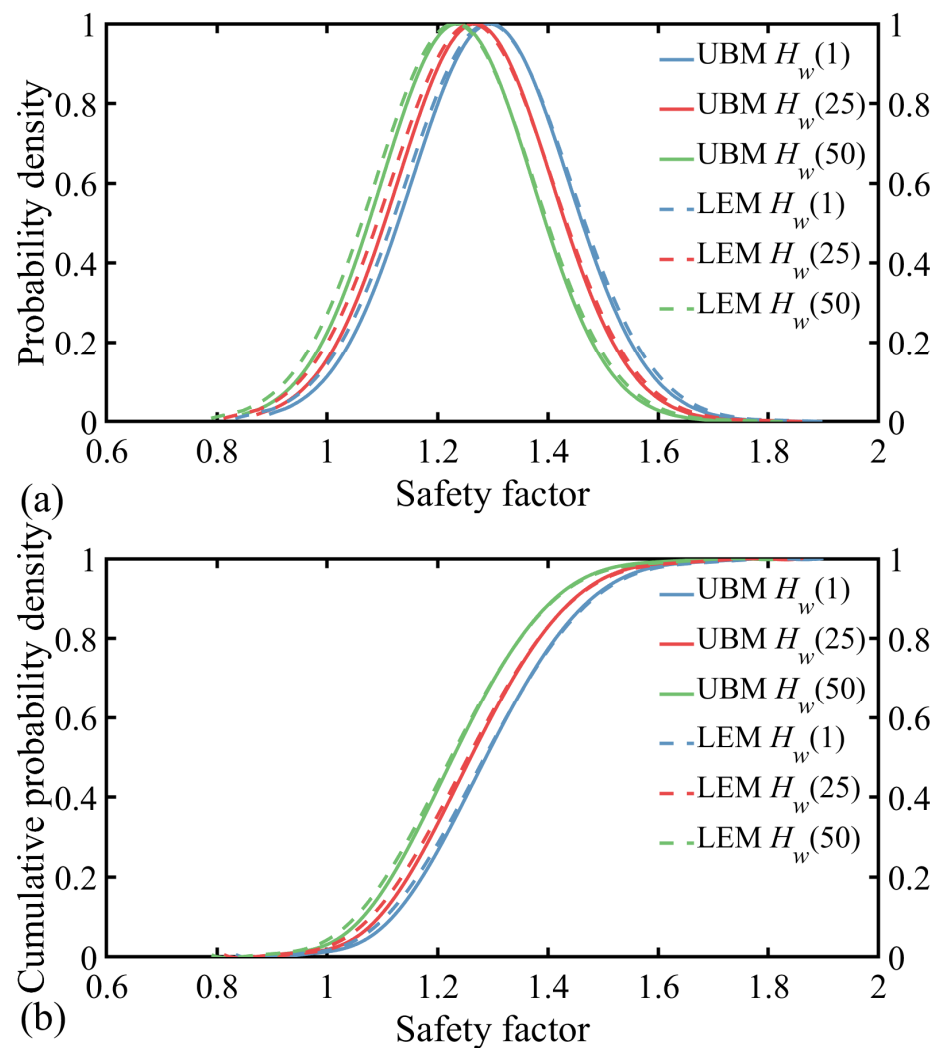


Figure 8. Distribution characteristics of the slope safety factors: (a) PDF curve of the safety factor; (b) CDF curve of the safety factor.

The calculation results show the following:

- (1) When $T_w = 1$, $T_w = 25$, and $T_w = 50$, the mean of the slope safety factors with the UBM is larger than that of the LEM, but the error is small, which conforms to the features of the upper bound solution. In addition, the slope safety factors acquired with the UBM and LEM methods decrease as the groundwater level rises. The slope failure probability increases acquired with the UBM and LEM decrease as the groundwater level rises. On the basis of the upper bound theorem, the slope safety factor acquired with the UBM must be greater than the real solution. Therefore, the UBM will slightly underestimate the failure slope probability.
- (2) Figure 8a,b shows the PDF and CDF curves of the slope safety factors acquired with the UBM and LEM under three groundwater level acts, $T_w = 1$, $T_w = 25$, and $T_w = 50$, respectively. It is not difficult to see that the PDF and CDF curves of the slope safety factors acquired with the UBM and LEM are very close with small errors. In addition, the PDF and CDF curves gradually move to the left as the groundwater level rises.
- (3) Figure 9a–c are the distribution histograms of the slope safety factors acquired with the UBM under the three groundwater level acts, $T_w = 1$, $T_w = 25$, and $T_w = 50$, respectively. It is not difficult to see that the distribution of the slope safety factors is similar to the stochastic groundwater levels.

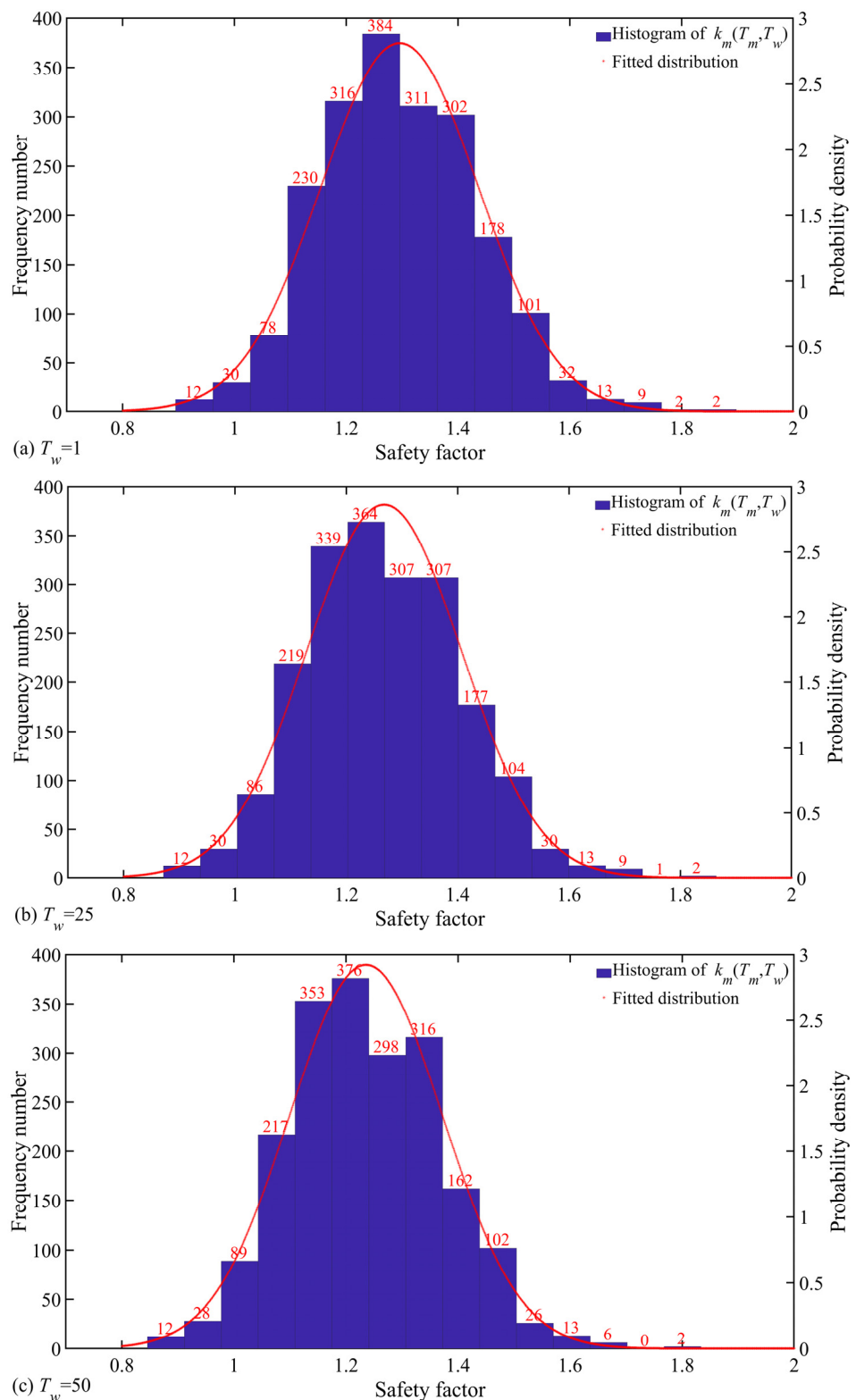


Figure 9. Distribution histograms of the slope safety factors: (a) $T_w = 1$; (b) $T_w = 25$; (c) $T_w = 50$.

On the basis of the stochastic programming model and solution strategy, the quantity of 100,000 slope safety factors was acquired. Figures 10 and 11 are the number of 50 PDF and CDF curves of the slope safety factors, respectively. Figure 12 reflects the mean and standard deviation of the slope safety factors versus the groundwater level. Figure 13

shows the PDF and CDF curves of the slope safety factors under all potential groundwater level acts acquired. The following rules can be acquired through analysis:

- (1) The distribution of the slope safety factors is consistent with the normal distribution. The mean of the slope safety factors tends to decrease as the groundwater level rises. The PDF and CDF curves of the slope safety factors gradually move to the left as the groundwater level rises. In addition, the standard deviation of the slope safety factor tends to decrease as the groundwater level rises. The range of the PDF curve and the trend of the CDF curve of the slope safety factors gradually narrow and steepen, respectively.
- (2) A polynomial fit is used to acquire the quantitative equation of the mean and standard deviation of the slope safety factors and groundwater level as follows:

$$u_k(T_w) = -0.0439H_w + 1.5963 \quad (28)$$

$$\sigma_k(T_w) = -0.0039H_w + 0.1685 \quad (29)$$

- (3) The quantity of 100,000 slope safety factors was acquired from 2000 stochastic fields under 50 groundwater level acts to perform the statistical analysis of all the acquired data; under 50 groundwater level acts, the mean and standard deviation of the slope safety factors are 1.2664 and 0.11, respectively.

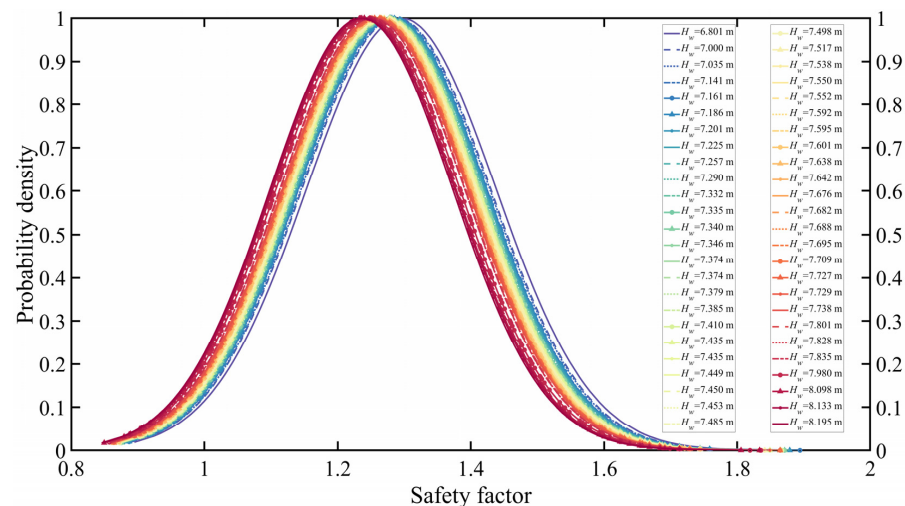


Figure 10. PDF curve of the slope safety factors.

Based on 100,000 Monte Carlo simulations of the slope, the LEM default is that only one failure mode exists (as shown in the LEM sliding surface in Figure 14). The biggest advantage of the UBM compared with the LEM in this paper is that all slope failure modes can be captured according to the failure information of the elements (as shown in the pink failure area in Figure 14) and then the reliability index for the slope can be calculated. Similar to the method in reference 37, the failure areas were used to classify the failure modes; there are six failure modes of the slope under 50 groundwater level acts (as shown in Figure 14). Table 3 lists the failure risk of the above six slope failure modes. Table 4 lists the failure risk corresponding to the failure modes when $T_w = 1$, $T_w = 25$, and $T_w = 50$. The results show that failure modes 1 and 2 have a small failure area that belongs to a shallow landslide, and the failure area is between 28.68 and 58.91 m² (failure times is 997). Failure modes 5 and 6 have a large failure area that belongs to a deep landslide, and the failure area is between 89.17 and 119.38 m² (failure times is 160). Failure modes 3 and 4 are between a shallow landslide and a deep landslide, and the failure area is between 58.91 and 89.04 m² (failure times is 989). When the groundwater level is $T_w = 1$, the slope has only

five failure modes; when the groundwater level is $T_w = 25$ and $T_w = 50$, the fifth failure modes occur. The phreatic line moves up, correspondingly, and the saturated area inside the slope increases as the groundwater level rises, thus increasing the probability of the failure mode.

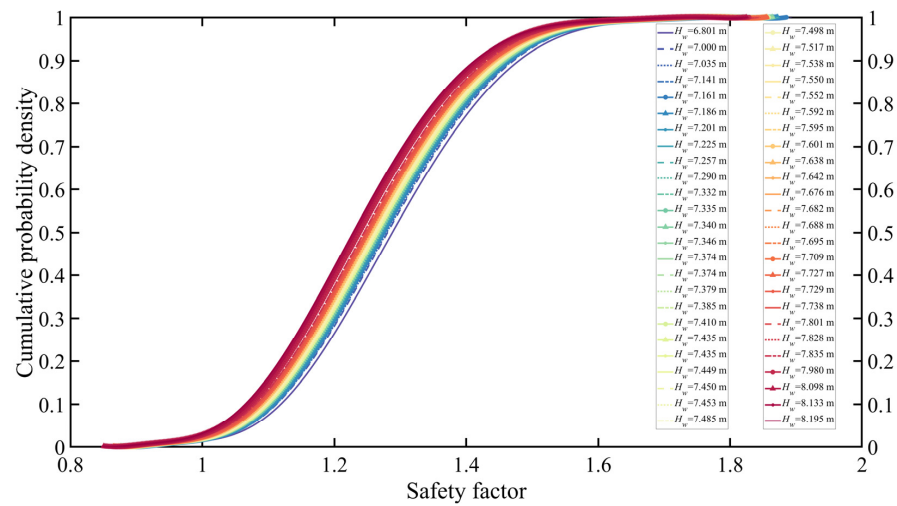
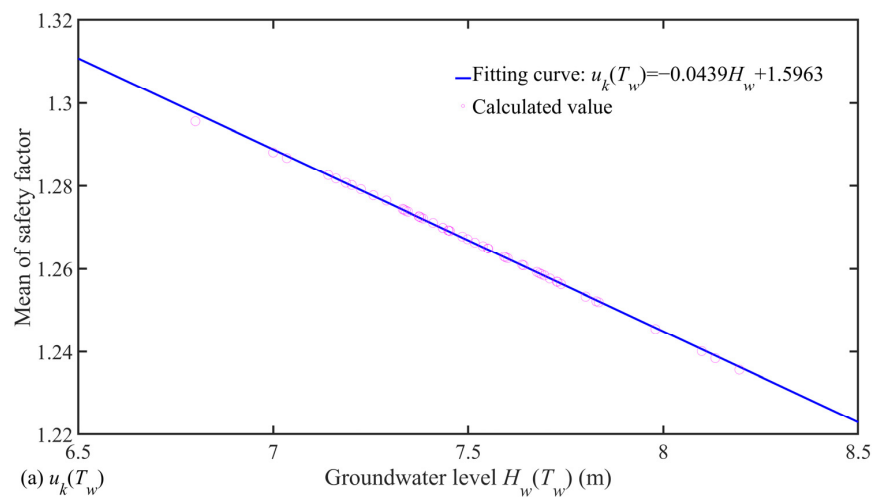
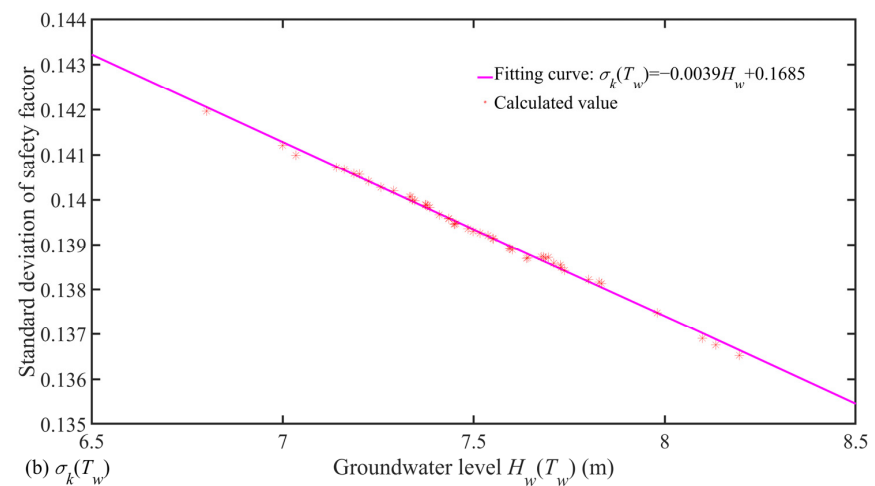


Figure 11. CDF curve of the slope safety factors.



(a) $u_k(T_w)$



(b) $\sigma_k(T_w)$

Figure 12. Slope safety factors versus groundwater level: (a) $u_k(T_w)$; (b) $\sigma_k(T_w)$.

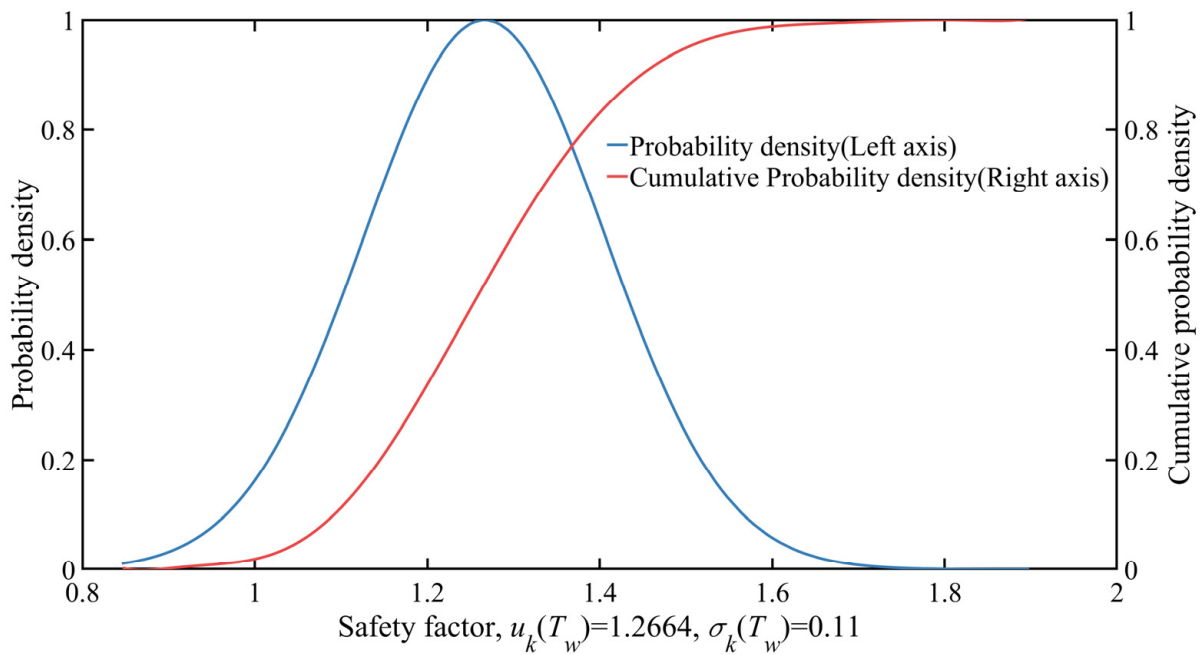


Figure 13. PDF and CDF curves of the slope safety factors under all potential groundwater level acts.

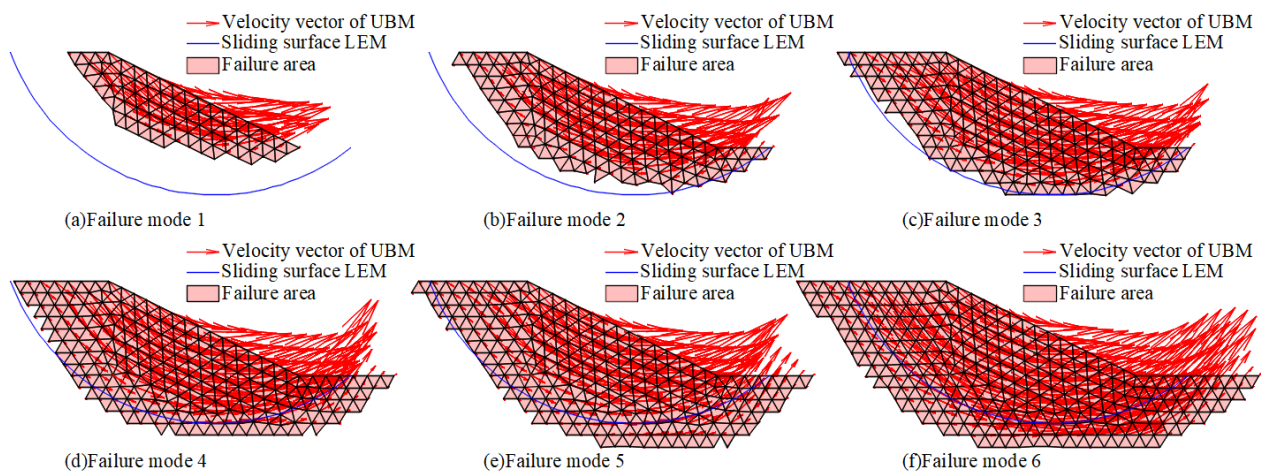


Figure 14. Schematic diagram results of the slope failure modes: (a) Failure mode 1; (b) Failure mode 2; (c) Failure mode 3; (d) Failure mode 4; (e) Failure mode 5; (f) Failure mode 6.

Table 3. Failure risk of the slope.

Failure Mode	Failure Area (m ²)	Failure Times	Failure Probability (%)	Failure Risk (m ²)
Mode 1	28.68–43.70	246	0.246	0.097
Mode 2	43.81–58.91	751	0.751	0.384
Mode 3	58.91–73.96	768	0.768	0.508
Mode 4	74.21–89.04	221	0.221	0.180
Mode 5	89.17–103.70	88	0.088	0.081
Mode 6	106.71–119.38	72	0.072	0.081
Sum	/	2146	2.146	1.332

The failure mode acquired with the LEM is only consistent with failure mode 3 in this paper. The main reason is that, when the LEM is adopted to calculate the slope safety factor, the initial slip surface is assumed in advance, then a constantly repeated search based on the mean of the shear parameters to acquire the critical slip crack surface is performed, and

then the slope safety factor is calculated based on the unique critical slip surface. Thus, a difference exists between the critical slip surface obtained with the LEM and the actual slip surface. The UBM constructs a stochastic programming model through finite elements, and then uses the method of stochastic mathematical programming to search the instability area of the slope, so the result is more in line with the real situation. The calculation indicates that the traditional LEM will ignore some failure modes and may miscalculate the slope failure risk, considering both the randomness of the groundwater level and soil shear strength parameters. The UBM can ignore the constitutive relation of the materials and acquire the slope safety factor and failure modes. Its applicability and calculation efficiency are both high.

Table 4. Failure risk of the slope when $T_w = 1$, $T_w = 25$, and $T_w = 50$.

Groundwater Level	Failure Mode	Failure Times	Failure Probability (%)	Failure Risk (m ²)
$T_w = 1$	Mode 1	3	0.15	0.057
	Mode 2	13	0.65	0.334
	Mode 3	10	0.50	0.342
	Mode 4	1	0.05	0.038
	Mode 6	1	0.05	0.057
$T_w = 25$	Mode 1	5	0.25	0.096
	Mode 2	14	0.70	0.366
	Mode 3	16	0.80	0.528
	Mode 4	5	0.25	0.210
	Mode 5	1	0.05	0.045
	Mode 6	1	0.05	0.056
$T_w = 50$	Mode 1	8	0.40	0.160
	Mode 2	19	0.95	0.490
	Mode 3	24	1.20	0.793
	Mode 4	11	0.55	0.445
	Mode 5	2	0.10	0.091
	Mode 6	2	0.10	0.115

Table 5 is the statistical table of the slope failure risk acquired with the three methods. The LEM default is that only one failure mode exists when $T_w = 1$, $T_w = 25$, and $T_w = 50$; the slope failure risk according to the LEM with Equation (12) is 1.121 m², 1.593 m², and 2.325 m², respectively. All failure modes can be acquired with the UBM. When $T_w = 1$, $T_w = 25$, and $T_w = 50$, the slope failure risk according to the UBM with Equation (14) and the UBM Equation (22) are 0.829 m², 1.302 m², and 2.094 m², respectively. It should be noted that Equation (14) has a difference calculation principle from Equation (22). All slope failure modes are required to be counted when Equation (14) is used to calculate the slope failure risk; the EFP for all elements is easy to acquire by solving Equation (5), and the element area is fixed when using Equation (22) to calculate the slope failure risk. From the calculation principle, the proposed method will simplify the calculation process and make the calculation more efficient.

Table 5. Failure risk statistical table of the slope (Unit: m²).

Groundwater	Method	LEM with Equation (12)	UBM with Equation (14)	UBM with Equation (22)
	$T_w = 1$		1.121	0.829
$T_w = 25$		1.593	1.302	1.302
$T_w = 50$		2.325	2.094	2.094

The EFP of the slope under T_w th groundwater level acts when $T_w = 1$, $T_w = 25$, and $T_w = 50$ obtained with Equation (18) is shown in Figure 15. The EFP of the slope under all potential groundwater level acts obtained with Equation (19) is shown in Figure 16. It can be observed that the groundwater level influences the EFP of the slope. The white area in the figure is the non-failure element, and the blue area is the failure element. In addition, according to the theory of EFP, the darker the color, the greater the EFP.

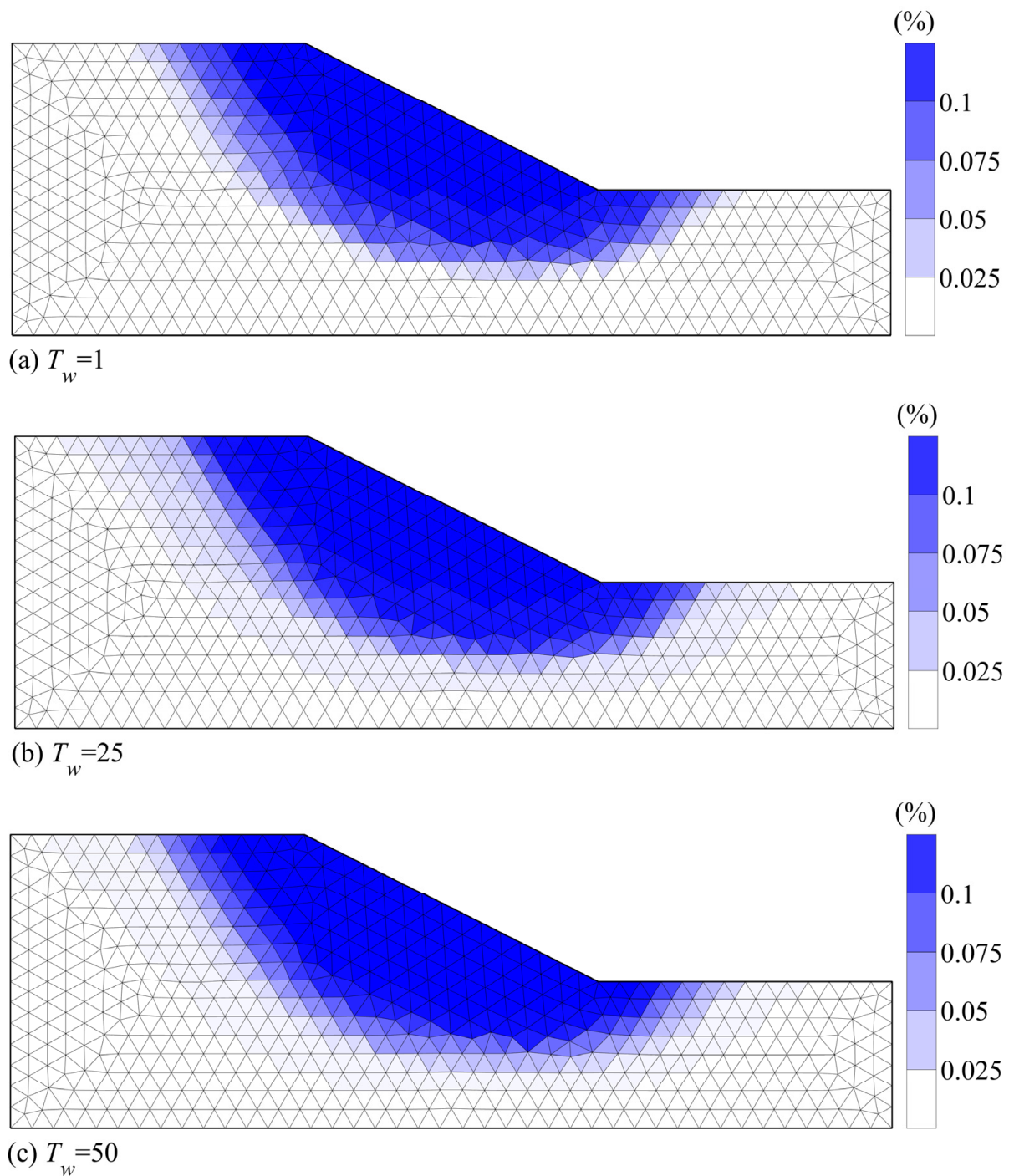


Figure 15. EFP of the slope under T_w th groundwater level acts: (a) $T_w = 1$; (b) $T_w = 25$; (c) $T_w = 50$.

The EFR of the slope under T_w th groundwater level acts when $T_w = 1$, $T_w = 25$, and $T_w = 50$ obtained with Equation (20) is shown in Figure 17. The EFR of the slope under all potential groundwater level acts obtained with Equation (21) is shown in Figure 18. It

can be observed that the groundwater level influences the EFR of the slope. When $T_w = 1$, the frequency of EFR between 0 and 0.00062 m² is 675, the frequency of EFR between 0.00062 and 0.00124 m² is 36, the frequency of EFR between 0.00124 and 0.00186 m² is 58, the frequency of EFR between 0.00186 and 0.00248 m² is 69, the frequency of EFR between 0.00248 and 0.00310 m² is 140, the frequency of EFR between 0.00310 and 0.00372 m² is 11, and the slope failure risk is 0.829 m². When $T_w = 25$, the frequency of EFR between 0 and 0.00082 m² is 670, the frequency of EFR between 0.00082 and 0.00164 m² is 32, the frequency of EFR between 0.00164 and 0.00246 m² is 54, the frequency of EFR between 0.00246 and 0.00328 m² is 56, the frequency of EFR between 0.00328 and 0.00410 m² is 165, the frequency of EFR between 0.00410 and 0.00492 m² is 12, and the slope failure risk is 1.302 m². When $T_w = 50$, the frequency of EFR between 0 and 0.00150 m² is 666, the frequency of EFR between 0.00150 and 0.00300 m² is 41, the frequency of EFR between 0.00300 and 0.00450 m² is 48, the frequency of EFR between 0.00450 and 0.00600 m² is 62, the frequency of EFR between 0.00600 and 0.00750 m² is 158, and the frequency of EFR between 0.00750 and 0.00900 m² is 14. Under all potential groundwater level acts, the frequency of EFR between 0 and 0.04820 m² is 674, the frequency of EFR between 0.04820 and 0.09640 m² is 30, and the frequency of EFR between 0.09640 and 0.14460 m² is 57. The frequency of EFR between 0.014460 and 0.19280 m² is 59, the frequency of EFR between 0.19280 and 0.24100 m² is 157, the frequency of EFR between 0.24100 and 0.28892 m² is 12, and the slope failure risk is 2.094 m². The element failure risk comprehensively reflects the contribution of the EFP and the element failure risk coefficient, which can make a quantitative judgment on the slope failure risk of each part. The slope failure risk is 1.332 m², obtained by the sum of all element failure risks. It is observed that the slope failure risk assessment method proposed in this paper can avoid the screening and statistical work of failure modes compared with the failure risk calculation results in Table 3.

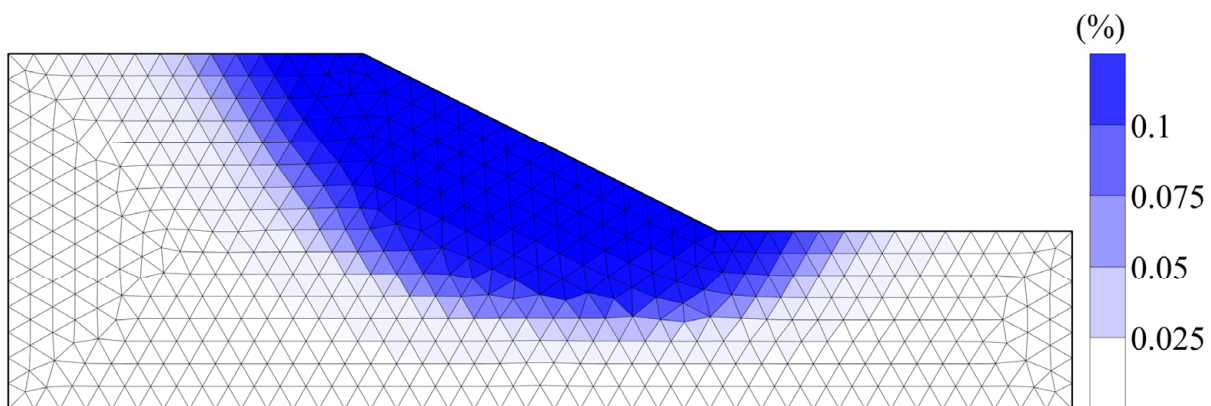


Figure 16. EFP of the slope under all potential groundwater level acts.

The safety performance decreases, and the IFP of the slope increases from 1.40% to 3.30% with the gradual increase in the groundwater level. Through cubic polynomial fitting, the IFP of the slope versus the groundwater level acquired (as shown in Figure 19) is as follows:

$$P_f^{IFP}(T_w) = 0.5271H_w^3 - 11.2957H_w^2 + 81.5794H_w - 196.7446 \quad (30)$$

The EFR of the slope increases from 0.829 m² to 2.094 m² with the gradual increase in the groundwater level. Through cubic polynomial fitting, the EFR of the slope versus the groundwater level acquired (as shown in Figure 20) is as follows:

$$R^{EFP}(T_w) = 0.1251H_w^3 - 2.4622H_w^2 + 16.6665H_w - 37.9602 \quad (31)$$

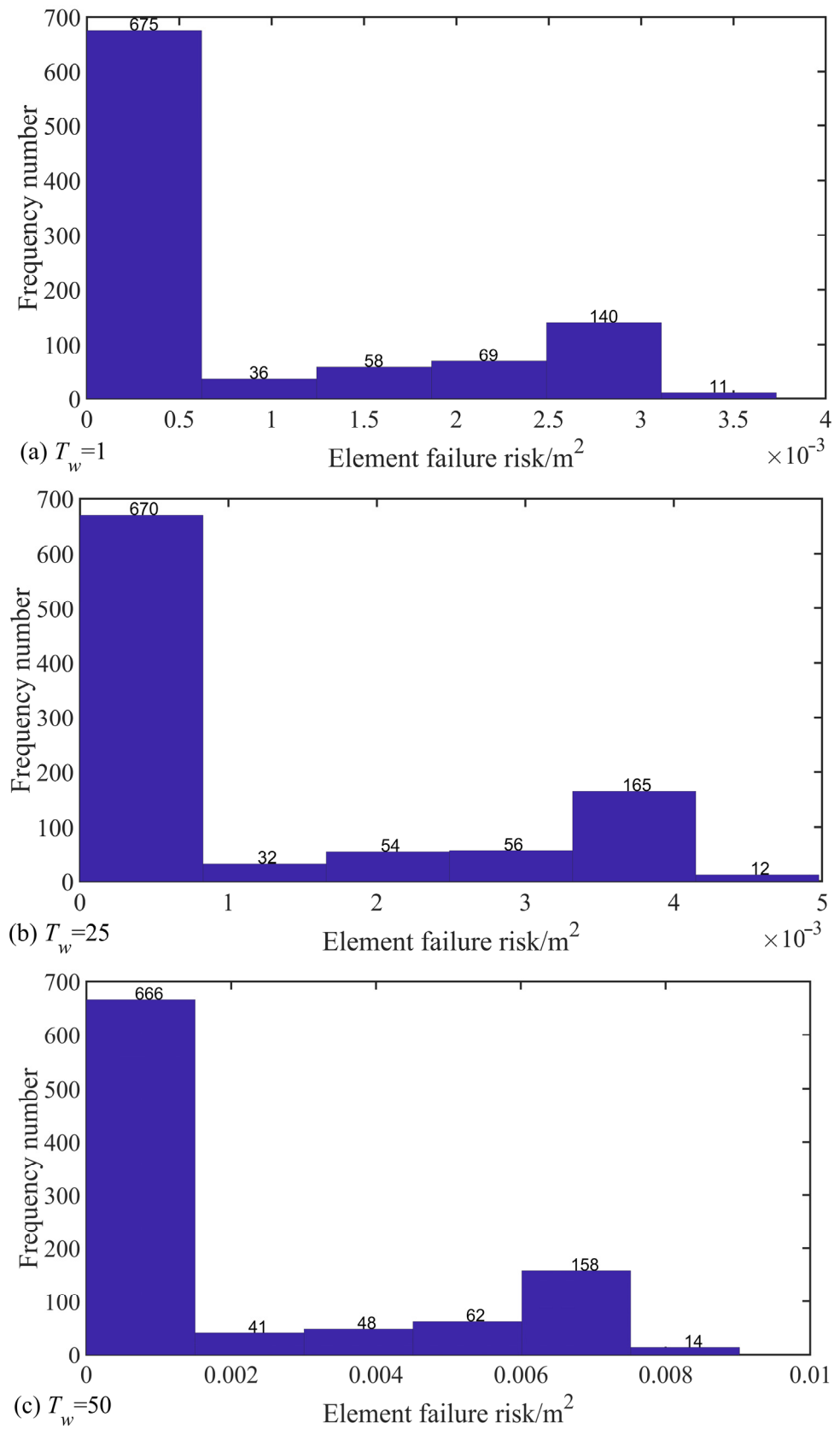


Figure 17. EFR of the slope under T_w th groundwater level acts: (a) $T_w = 1$; (b) $T_w = 25$; (c) $T_w = 50$.

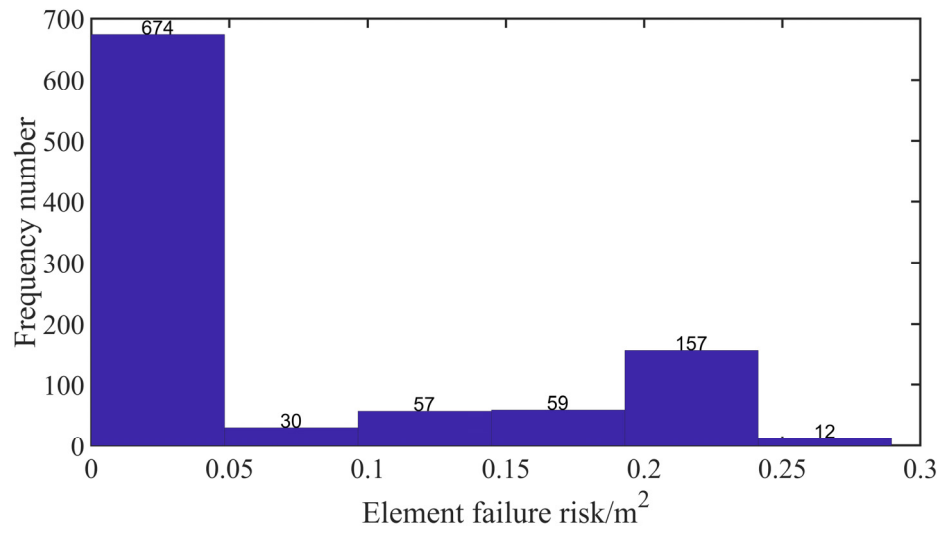


Figure 18. EFR of the slope under all potential groundwater level acts.

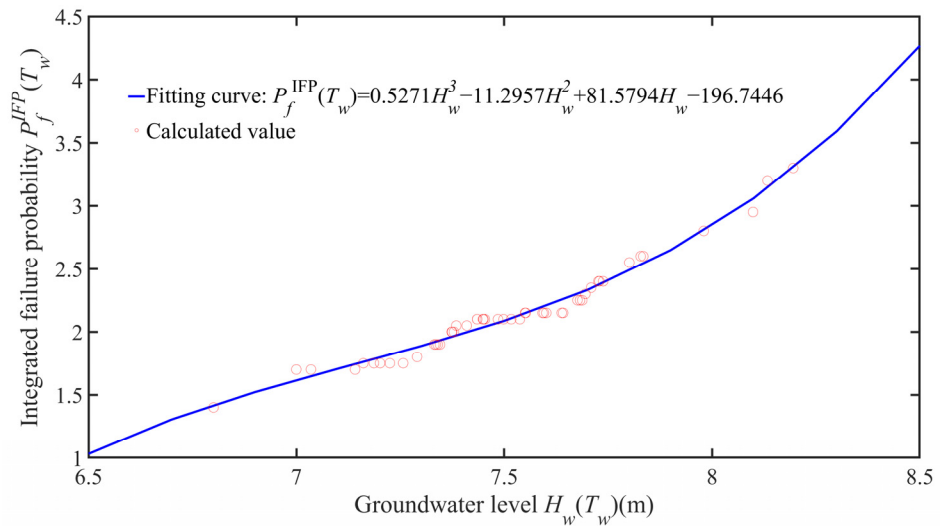


Figure 19. IFP of the slope versus the groundwater level (Unit: %).

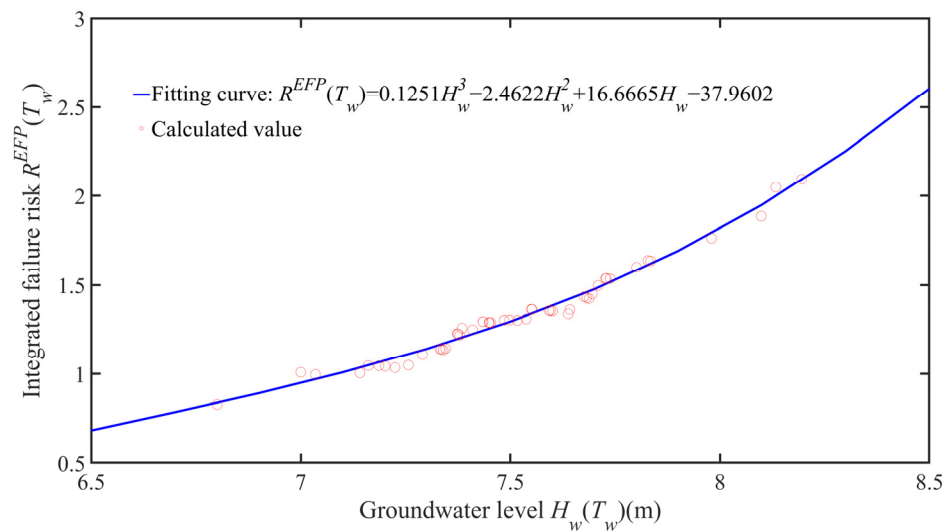


Figure 20. EFR of the slope versus the groundwater level (Unit: m²).

6. Conclusions

A slope failure risk assessment method that considers both the randomness of the groundwater level and soil shear strength parameters is proposed in this paper. The corresponding calculation program is compiled. The major conclusions are the following:

- (1) When the randomness of the groundwater level and soil shear strength parameters are considered comprehensively, the traditional LEM will ignore multiple failure modes and may miscalculate the slope failure risk. However, all failure modes can be acquired with the UBM for seeking the minimum value of the KAVF. Thus, the result is more consistent with the real situation. In addition, the traditional LEM only judges the slope stability by the safety factor, which only reflects the degree of the IPF. The EFP is used to calculate the EFR of the slope, which cannot only reflect the degree of the IPF but, also, the slope failure risk can be accurately acquired. It should be noted that this calculation method can greatly reduce the calculation cost.
- (2) The IPF and EFR of the slope are increasing from 1.40% to 3.30% and 0.829 m² to 2.094 m² with the rise of the groundwater level, respectively. Based on the EFP, the proposed method can accurately obtain the EFR of the slope under each groundwater level act by using the element's location information and failure situation. This will provide engineers with realistic reference values for the slope reinforcement design to achieve sustainable development.
- (3) Groundwater level and earthquakes are two important causes of slope instability and failure. However, this study does not consider the impact of earthquakes on slope reliability. Therefore, relevant studies on seismic slope stability will be carried out in the future. In addition, according to the upper bound theory, the upper bound solution is inevitably greater than the true solution. Therefore, the failure probability will be underestimated when using the UBM for slope reliability analysis. To solve this problem, there is a necessity to study the slope reliability calculation method on the basis of the lower bound theory in future research work. The solution of slope failure probability with the UBM and LBM can be obtained at the same time, so the interval range of the real failure probability can be accurately judged, and the reliability index of the slope can be quantified more accurately.

Author Contributions: Conceptualization, P.P., Z.L., X.Z., W.L., S.S. and H.X.; methodology, P.P.; software, Z.L.; validation, W.L.; formal analysis, Z.L.; investigation, Z.L.; resources, W.L.; data curation, W.L.; writing—original draft preparation, Z.L.; writing—review and editing, P.P.; visualization, H.X.; supervision, W.L. and Z.L.; project administration, S.S. and Z.L.; funding acquisition, X.Z. and Z.L. All authors have read and agreed to the published version of the manuscript.

Funding: This research was funded by the National Natural Science Foundation of China grant number 12162018 and 12262016; the Research Foundation of Science and technology plan project of Yunnan Provincial Department of Science and Technology grant number 202201AT070283 and 202305AD160064.

Institutional Review Board Statement: Not applicable for studies not involving humans or animals.

Informed Consent Statement: Not applicable.

Data Availability Statement: Not applicable.

Conflicts of Interest: The authors declare no conflict of interest.

References

1. Dai, F.; Lee, C.; Ngai, Y. Landslide risk assessment and management: An overview. *Eng. Geol.* **2002**, *64*, 65–87. [[CrossRef](#)]
2. Li, D.-Q.; Yang, Z.-Y.; Cao, Z.-J.; Zhang, L.-M. Area failure probability method for slope system failure risk assessment. *Comput. Geotech.* **2018**, *107*, 36–44. [[CrossRef](#)]
3. Liu, X.; Li, D.-Q.; Cao, Z.-J.; Wang, Y. Adaptive Monte Carlo simulation method for system reliability analysis of slope stability based on limit equilibrium methods. *Eng. Geol.* **2020**, *264*, 105384. [[CrossRef](#)]
4. Wang, L.; Wu, C.; Li, Y.; Liu, H.; Zhang, W.; Chen, X. Probabilistic Risk Assessment of unsaturated Slope Failure Considering Spatial Variability of Hydraulic Parameters. *KSCE J. Civ. Eng.* **2019**, *23*, 5032–5040. [[CrossRef](#)]

5. Malkawi, A.I.H.; Hassan, W.F.; Abdulla, F.A. Uncertainty and reliability analysis applied to slope stability. *Struct. Saf.* **2000**, *22*, 161–187. [[CrossRef](#)]
6. Zhao, H.-B. Slope reliability analysis using a support vector machine. *Comput. Geotech.* **2008**, *35*, 459–467. [[CrossRef](#)]
7. Ching, J.; Phoon, K.-K.; Hu, Y.-G. Efficient Evaluation of Reliability for Slopes with Circular Slip Surfaces Using Importance Sampling. *J. Geotech. Geoenviron. Eng.* **2009**, *135*, 768–777. [[CrossRef](#)]
8. Tang, X.-S.; Li, D.-Q.; Chen, Y.-F.; Zhou, C.-B.; Zhang, L.-M. Improved knowledge-based clustered partitioning approach and its application to slope reliability analysis. *Comput. Geotech.* **2012**, *45*, 34–43. [[CrossRef](#)]
9. Cho, S.E. First-order reliability analysis of slope considering multiple failure modes. *Eng. Geol.* **2013**, *154*, 98–105. [[CrossRef](#)]
10. Ji, J.; Zhang, W.; Zhang, F.; Gao, Y.; Lü, Q. Reliability analysis on permanent displacement of earth slopes using the simplified Bishop method. *Comput. Geotech.* **2020**, *117*, 103286. [[CrossRef](#)]
11. Wang, W.; Li, D.-Q.; Liu, Y.; Du, W. Influence of ground motion duration on the seismic performance of earth slopes based on numerical analysis. *Soil Dyn. Earthq. Eng.* **2021**, *143*, 106595. [[CrossRef](#)]
12. Griffiths, D.V.; Huang, J.; Fenton, G.A. Influence of Spatial Variability on Slope Reliability Using 2-D Random Fields. *J. Geotech. Geoenviron. Eng.* **2009**, *135*, 1367–1378. [[CrossRef](#)]
13. Shen, H.; Abbas, S.M. Rock slope reliability analysis based on distinct element method and random set theory. *Int. J. Rock Mech. Min. Sci.* **2013**, *61*, 15–22. [[CrossRef](#)]
14. Li, D.-Q.; Jiang, S.-H.; Cao, Z.-J.; Zhou, W.; Zhou, C.-B.; Zhang, L.-M. A multiple response-surface method for slope reliability analysis considering spatial variability of soil properties. *Eng. Geol.* **2015**, *187*, 60–72. [[CrossRef](#)]
15. Wang, M.-Y.; Liu, Y.; Ding, Y.-N.; Yi, B.-L. Probabilistic stability analyses of multi-stage soil slopes by bivariate random fields and finite element methods. *Comput. Geotech.* **2020**, *122*, 103529. [[CrossRef](#)]
16. Dyson, A.P.; Tolooiyan, A. Comparative Approaches to Probabilistic Finite Element Methods for Slope Stability Analysis. *Simul. Model. Pract. Theory* **2020**, *100*, 102061. [[CrossRef](#)]
17. Lysmer, J. Limit Analysis of Plane Problems in Soil Mechanics. *J. Soil Mech. Found. Div.* **1970**, *96*, 1311–1334. [[CrossRef](#)]
18. Li, Z.; Chen, Y.; Guo, Y.; Zhang, X.; Du, S. Element Failure Probability of Soil Slope under Consideration of Random Groundwater Level. *Int. J. Géoméch.* **2021**, *21*, 04021108. [[CrossRef](#)]
19. Sloan, S.W. Lower bound limit analysis using finite elements and linear programming. *Int. J. Numer. Anal. Methods Géoméch.* **1988**, *12*, 61–77. [[CrossRef](#)]
20. Sloan, S.; Kleeman, P. Upper bound limit analysis using discontinuous velocity fields. *Comput. Methods Appl. Mech. Eng.* **1995**, *127*, 293–314. [[CrossRef](#)]
21. Li, Z.; Hu, Z.; Zhang, X.; Du, S.; Guo, Y.; Wang, J. Reliability analysis of a rock slope based on plastic limit analysis theory with multiple failure modes. *Comput. Geotech.* **2019**, *110*, 132–147. [[CrossRef](#)]
22. Kim, J.; Salgado, R.; Yu, H.S. Limit Analysis of Soil Slopes Subjected to Pore-Water Pressures. *J. Geotech. Geoenviron. Eng.* **1999**, *125*, 49–58. [[CrossRef](#)]
23. Li, Z.; Zhou, Y.; Guo, Y. Upper-Bound Analysis for Stone Retaining Wall Slope Based on Mixed Numerical Discretization. *Int. J. Géoméch.* **2018**, *18*, 04018122. [[CrossRef](#)]
24. Liu, W.; Xu, H.; Sui, S.; Li, Z.; Zhang, X.; Peng, P. Lower Bound Limit Analysis of Non-Persistent Jointed Rock Masses Using Mixed Numerical Discretization. *Appl. Sci.* **2022**, *12*, 12945. [[CrossRef](#)]
25. Chen, Z.H.; Lei, J.; Huang, J.H.; Cheng, X.H.; Zhang, Z.C. Finite element limit analysis of slope stability considering spatial variability of soil strengths. *Chin. J. Geotech. Eng.* **2018**, *40*, 985–993. [[CrossRef](#)]
26. Peng, P.; Li, Z.; Zhang, X.Y.; Shen, L.F.; Xu, Y. Research on element failure probability and failure mode of soil slope. *Eng. Mech.* **2022**, *39*, 1–15. [[CrossRef](#)]
27. Silva, F.; Lambe, T.W.; Marr, W.A. Probability and Risk of Slope Failure. *J. Geotech. Geoenviron. Eng.* **2008**, *134*, 1691–1699. [[CrossRef](#)]
28. Cassidy, M.J.; Uzielli, M.; Lacasse, S. Probability risk assessment of landslides: A case study at Finneidfjord. *Can. Geotech. J.* **2008**, *45*, 1250–1267. [[CrossRef](#)]
29. Zhang, X.Y.; Zhang, L.X.; Li, Z. Reliability analysis of soil slope based on upper bound method of limit analysis. *Rock Soil Mech.* **2018**, *39*, 1840–1850. [[CrossRef](#)]
30. Zuo, Z.; Zhang, L.; Cheng, Y.; Wang, J.; He, Y. Probabilistic back analysis of unsaturated soil seepage parameters based on Markov chain Monte Carlo method. *Rock Soil Mech.* **2013**, *34*, 2393–2400.
31. Wang, X.; Xia, X.; Zhang, X.; Gu, X.; Zhang, Q. Probabilistic Risk Assessment of Soil Slope Stability Subjected to Water Drawdown by Finite Element Limit Analysis. *Appl. Sci.* **2022**, *12*, 10282. [[CrossRef](#)]
32. Cho, S.E.; Park, H.C. Effect of spatial variability of cross-correlated soil properties on bearing capacity of strip footing. *Int. J. Numer. Anal. Methods Géoméch.* **2010**, *34*, 1–26. [[CrossRef](#)]
33. Shadabfar, M.; Huang, H.; Kordestani, H.; Muho, E.V. Reliability Analysis of Slope Stability Considering Uncertainty in Water Table Level. *ASCE-ASME J. Risk Uncertain. Eng. Syst. Part A Civ. Eng.* **2020**, *6*, 04020025. [[CrossRef](#)]
34. Li, K.S.; Lumb, P. Probabilistic design of slopes. *Can. Geotech. J.* **1987**, *24*, 520–535. [[CrossRef](#)]
35. Li, D.Q.; Jiang, S.H.; Zhou, C.B.; Phoon, K.K. Reliability analysis of slopes considering spatial variability of soil parameters using non-intrusive stochastic finite element method. *Chin. J. Geotech. Eng.* **2013**, *35*, 1413–1421.

36. Zhou, J.; Qin, C. Stability analysis of unsaturated soil slopes under reservoir drawdown and rainfall conditions: Steady and transient state analysis. *Comput. Geotech.* **2022**, *142*, 104541. [[CrossRef](#)]
37. Huang, J.; Lyamin, A.; Griffiths, D.V.; Krabbenhoft, K.; Sloan, S. Quantitative risk assessment of landslide by limit analysis and random fields. *Comput. Geotech.* **2013**, *53*, 60–67. [[CrossRef](#)]

Disclaimer/Publisher’s Note: The statements, opinions and data contained in all publications are solely those of the individual author(s) and contributor(s) and not of MDPI and/or the editor(s). MDPI and/or the editor(s) disclaim responsibility for any injury to people or property resulting from any ideas, methods, instructions or products referred to in the content.